Homeostatic plasticity shapes the retinal response to photoreceptor degeneration

Ning Shen[1], **Bing Wang**[1], **Florentina Soto**[1], **Daniel Kerschensteiner**[1,2,3,4,5,*]

[1]John F. Hardesty, MD Department of Ophthalmology and Visual Sciences, Washington University School of Medicine, 660 S. Euclid Ave., Saint Louis, MO 63110, USA

[2]Department of Neuroscience, Washington University School of Medicine, 660 S. Euclid Ave., Saint Louis, MO 63110, USA

[3]Department of Biomedical Engineering, Washington University School of Medicine, 660 S. Euclid Ave., Saint Louis, MO 63110, USA

[4]Hope Center for Neurological Disorders, Washington University School of Medicine, 660 S. Euclid Ave., Saint Louis, MO 63110, USA

[5]Lead Contact

SUMMARY

Homeostatic plasticity stabilizes input and activity levels during neural development, but whether it can restore connectivity and preserve circuit function during neurodegeneration is unknown. Photoreceptor degeneration is the most common cause of blindness in the industrialized world. Visual deficits are dominated by cone loss, which progresses slowly, leaving a window during which rewiring of second-order neurons (i.e., bipolar cells) could preserve function. Here, we establish a transgenic model to induce cone degeneration with precise control and analyze bipolar cell responses and their impact on vision through anatomical reconstructions, *in vivo* electrophysiology, and behavioral assays. In young retinas, we find that three bipolar cell types precisely restore input synapse numbers when 50% of cones degenerate, but one does not. Of the three bipolar cell types that rewire, two contact new cones within stable dendritic territories, whereas one expands its dendrite arbors to reach new partners. In mature retinas, only one of four bipolar cell types rewires homeostatically. This steep decline in homeostatic plasticity is accompanied by reduced light responses of bipolar cells and deficits in visual behaviors. By contrast, light responses and behavioral performance are preserved when cones degenerate in young mice. Our results reveal unexpected cell-type specificity and a steep maturational decline of


DECLARATION OF INTERESTS

The authors declare no competing financial interests.

homeostatic plasticity. The impact of homeostatic plasticity on functional outcomes identify it as a promising therapeutic target for retinal and other neurodegenerative diseases.

eTOC blurb

Shen *et al.* find that homeostatic plasticity in young retinas differ between closely related bipolar cell types in the retina, that homeostatic plasticity of bipolar cells declines steeply with age, and that it determines the visual deficits incurred from photoreceptor degeneration.

Graphical Abstract
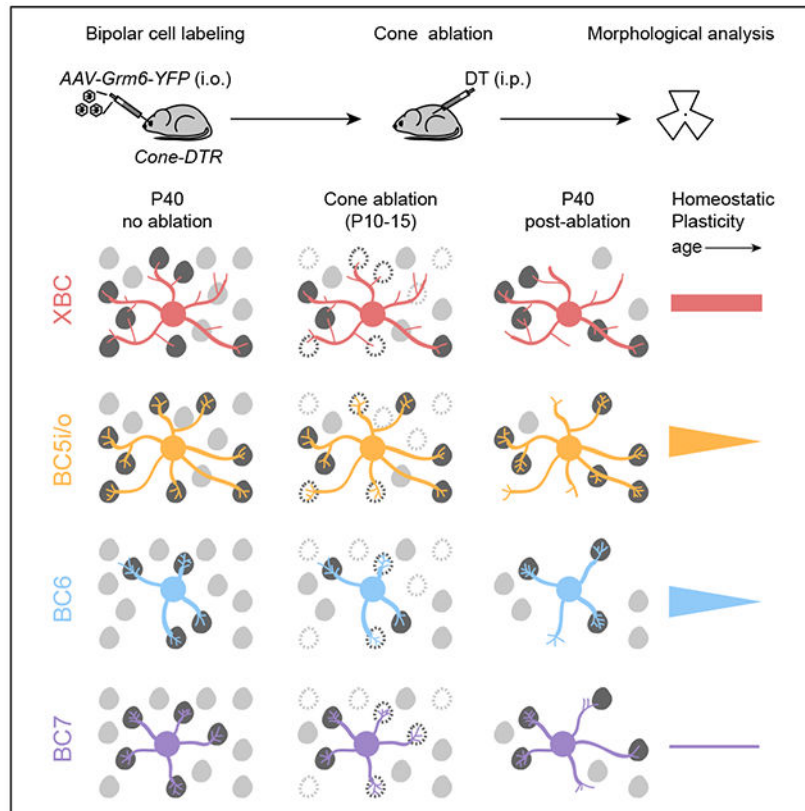
INTRODUCTION

Homeostatic plasticity refers to the neuronal drive to return to a functional setpoint and the mechanisms by which this goal is accomplished [1-3]. Homeostatic plasticity can regulate many aspects of neuronal morphology, connectivity, and function, but exerts particularly powerful control over dendrites and their synapses [4,5]. During development, neurons can stabilize input by expanding dendrites when synaptic partners are scarce [6], by recruiting new synaptic partners when the regular ones are missing or dysfunctional [7], and by adjusting the number of synapses with each partner in inverse proportion to the total number of partners contacted [4,7,8]. In neurodegeneration, neurons gradually lose input partners. To what extent homeostatic plasticity can counteract this loss is unknown. This is in part because it is unclear how homeostatic plasticity changes with age. Numerous cell-type-

specific cues guide the assembly of precise circuits from diverse components [9]. How the homeostatic mechanisms that stabilize and maintain circuits differ between neurons has not been explored. Here, we study how homeostatic plasticity shapes the responses of retinal bipolar cells to photoreceptor degeneration, examining changes with age and differences between cell types.

Bipolar cells are glutamatergic second-order neurons of the visual system, which relay photoreceptor (i.e., rod and cone) signals from the outer retina to amacrine and ganglion cells in the inner retina [10]. There are 15 types of bipolar cells in mice [11,12]. One exclusively contacts rods, which function in dim light, and 14 contact cones, which function in bright light and dominate vision in the modern world [13]. Most bipolar cell types are conserved from rodents to primates [14]. Photoreceptor degeneration is the leading cause of blindness in industrialized countries [15]. It can be divided into monogenic inherited retinal degenerations (IRDs), in which mutations in one of more than 300 genes cause photoreceptor death [16], and age-related macular degeneration (AMD), a genetically complex multifactorial disease [17]. Cones can be the primary target of photoreceptor degeneration or perish when they lose trophic support from rods [18,19]. In AMD and many IRDs, cone loss progresses slowly, leaving a window of opportunity during which homeostatic plasticity of bipolar cell dendrites could preserve visual function [17,20].

Studying bipolar cell plasticity in mouse models that implement human IRD and AMD mutations is complicated by mixed and variable rod and cone loss [21-23]. Furthermore, progressive photoreceptor degeneration precludes comparisons of plasticity across age. Previous studies of responses to partial cone loss revealed remodeling of bipolar cell dendrites [24-26]. However, whether dendritic remodeling restores synapses with the quantitative accuracy characteristic of homeostatic plasticity, how plasticity differs between bipolar cell types, and how it changes with age is unknown. Finally, the therapeutic potential of homeostatic plasticity depends on its ability to improve the functional outcomes of neurodegeneration. This remains untested.

Here, we establish a transgenic model that allows for precise control of cone degeneration [24]. We selectively remove 50% of cones in young and mature mice, compare dendritic remodeling and synaptic rewiring of four bipolar cell types in response to these manipulations, and relate differences in homeostatic plasticity to differences in bipolar cell function and visual behaviors.

RESULTS

Precise control of cone degeneration in *Cone-DTR* mice

To control the timing and extent of cone degeneration, we crossed transgenic mice expressing Cre recombinase in cones (*Cone-Cre* mice) [27] to mice expressing the diphtheria toxin receptor Cre dependently from a ubiquitously active locus (*DTR* mice) [28]. We injected double-positive offspring (*Cone-DTR* mice) intraperitoneally with diphtheria toxin (DT) at postnatal day 10 (P10, young mice) or P30 (mature mice), titrating until we reached concentrations that eliminated half the cones. Cone degeneration was selective, swift, and stationary. Cone density was reduced three days post DT injection and remained

stable thereafter (Figure 1A-D, G-J). Rod photoreceptors and other retinal neurons, including bipolar cells, were unaffected (Figure 1M-O, S-U, and Figure S1) [24]. Bipolar cells contact two types of cones: M-cones, which express a mixture of medium- (M-) and short-wavelength-sensitive (S-) opsins [29-31], and S-cones, which express only S-opsin. Cone degeneration affected M- and S-cones equally (Figure 1P-R, and V-X), and we, therefore, combined them in our subsequent analysis. The presynaptic terminals (i.e., pedicles) of cones enlarged when their density was reduced (Figure 1A, D, F, G, J, L). This pedicle hypertrophy was similar for cone degeneration in young and mature mice (Figure 1F, L). Throughout our study, we used *Cone-Cre* and *DTR* mice injected with DT as controls. Thus, we established a transgenic model to induce cone degeneration with precise control and observed presynaptic plasticity in young and mature mice.

Identification of bipolar cell types by stable axon morphologies

Of the 14 bipolar cell types that contact cones, the *Grm6* promoter is active in eight, which depolarize to light increments (i.e., ON bipolar cells). In our study, we focused on the four of these that were most reliably labeled by *AAV-Grm6-YFP* [4,5]: XBC, BC5i/o, BC6, and BC7. Bipolar cell axons stratify at distinct depths within the retina's inner plexiform layer (IPL) and differ in size and branching patterns [32]. Staining for ChAT labels the dendrites of ON and OFF starburst amacrine cells, which stratify in two narrow bands (i.e., ChAT bands) commonly used as markers of IPL stratification. XBC and BC5i/o stratify above the inner ChAT band (Figure 2A, H) with large sparsely branched axons and small densely branched axons, respectively (Figure 2D, K, and Figure S2). BC5i/o combines two cell types that are morphologically identical, but whose axons form separate tiled arrays [33]. We distinguished BC5i/o cells from rarely labeled BC5t cells by their monostratified arbors (Figure S2). BC6 and BC7 axons stratify broadly and narrowly, respectively, below, the inner ChAT band (Figure 2O, V). In some of our experiments, BC6 and BC7 cells were labeled by transgenic expression of tdTomato (*Grm6-tdTomato* mice) [34]. Results from these experiments were indistinguishable from those of viral labeling and were therefore combined with them. Comparing *Cone-DTR* and control mice injected with DT at postnatal day 10 (P10) at P40, showed that cone loss in young retinas did not affect bipolar cell axon stratification profiles (Figure 2A-C, H-J, O-Q, V-X). Furthermore, axon size and synapse numbers, counted after masking immunostaining for C-terminal binding protein 2 (CtBP2) by the viral fluorescent labeling, differed widely between bipolar cell types but were indistinguishable between *Cone-DTR* and control retinas (Figure 2D-G, K-N, R-U, Y-B'). Thus, bipolar cell axons and output synapses remain stable after cone degeneration. We, therefore, used bipolar cell axon size, branching, stratification, and connectivity patterns to assign bipolar cells to specific types.

Homeostatic plasticity of bipolar cell dendrites in young mice

Much is known about the cell-type-specific molecular cues and developmental strategies that dendrites follow to establish unique patterns of connectivity [9,35]. By contrast, how the homeostatic mechanisms that maintain and restore connectivity differ between neuron types is unclear. To compare dendritic responses to cone degeneration in young mice, we sparsely labeled bipolar cells by intravitreal injection of *AAV-Grm6-YFP* in P6 *Cone-DTR* pups,

induced cone degeneration by intraperitoneal DT injection at P10, and isolated retinas for morphological analysis at P40 (Figure 3A).

To assess the homeostatic plasticity of bipolar cells, we analyzed their dendrites' ability to restore input synapses following partial cone loss. Cone pedicles contain multiple ribbon release sites, and individual bipolar cell dendrites can form multiple invaginating synapses with a single cone [8,35,36]. Super-resolution imaging of retinal flat mounts with virally labeled bipolar cells, cone terminals stained for cone arrestin, and postsynaptic specializations of bipolar cells stained for Gpr179, a postsynaptic orphan receptor that, via the extracellular matrix protein pikachurin, interacts transsynaptically with dystroglycan and anchors regulators of G protein signaling near postsynaptic receptors [37,38], showed that more than 80% of dendritic tips of XBC, BC5i/o, BC6, and BC7 cells within cone terminals were synaptically differentiated (Figure S3). This percentage was indistinguishable between *Cone-DTR* and control mice (Figure S3). We, therefore, used bipolar cell dendrite tips within cone pedicles as a proxy for input synapses in the remainder of this study. Counting bipolar cell dendrite tips in pedicles revealed that despite losing 50% of cones to degeneration, dendrites of XBC (Figure 3B-D), BC5i/o (Figure 3H-J), and BC6 (Figure 3N-P) cells had precisely restored cone input synapse numbers 30 days after DT injection. BC7 cells failed to make a complete recovery from input loss (Figure 3T-V), indicating that the extent of homeostatic plasticity can differ between closely related neuron types.

We observed some Gpr179 clusters on bipolar cell dendrites outside of cone pedicles. Across all cell types examined, these clusters were rare in control and more frequent in *Cone-DTR* retinas (Figure S3), indicating that cone bipolar cell dendrites can contact rods when cones degenerate [39]. However, in our partial cone degeneration model, putative synapses with rods accounted for a small fraction of the overall input to cone bipolar cells (Figure S3).

We next compared the strategies by which bipolar cell dendrites restored synapses with cones. Both XBC and BC5i/o cells retained stable dendrite territories (Figure 3G, M), but contacted a larger fraction of cones within these territories (i.e., cone contact ratio, Figure 3F, L). In addition, they upregulated the number of dendritic tips penetrating each cone pedicle (Figure 3E, K). BC6 cells, which in control retinas already contact most of the cones in their dendritic fields (Figure 3R) [36], expanded territories to reach new cones (Figure 3S) and formed more synapses with each (Figure 3Q). The dendrites of BC7 cells expanded (Figure 3Y), penetrated each cone with more tips (Figure 3W), but did not contact significantly more cones within their dendritic territories (Figure 3X), and fell short of restoring input synapse numbers to pre-degeneration levels (Figure 3V). Across all types, rewiring varied gradually with cone loss (Figure S4). Thus, in young mice, homeostatic plasticity enables bipolar cells to regain inputs lost to cone degeneration. The extent and mechanisms of homeostatic rewiring differ between cell types.

Dendritic remodeling precedes synaptic rewiring

Seven days after P10 DT injections (Figure S5A, B, C, H, I, N, O, T, U), cone contact ratios were unchanged for all bipolar cell types examined (Figure S5F, L, R, X), and only BC5i/o cells had begun to upregulate their connectivity with individual cones (Figure S5E, K, Q,

W). Consequently, XBC, BC5i/o, BC6, and BC7 all had fewer input synapses in *Cone-DTR* than in control retinas (Figure S5D, J, P, V) at this time point (i.e., P17). Intriguingly, however, dendritic territories were enlarged for XBC, and BC5i/o as well as BC6 cells (Figure S5G, M, S).To probe whether the transient dendritic expansion of XBC and BC5i/o cells contributed to their subsequent synaptic rewiring, we compared the distances from bipolar cell bodies to the farthest cones contacted by their dendrites between *Cone-DTR* mice and simulations in which cone contacts were randomly removed from control dendrites (see STAR Methods). Based on this analysis, we conclude that whereas the stable dendritic expansion of BC6 cells recruited new cone partners (distance to the farthest cone in *Cone-DTR*: 13.71 ± 0.63 μm, in the simulation: 10.44 ± 0.41 μm, p = 0.002 by Mann–Whitney U test), the transient expansion of XBC (distance to the farthest cone in *Cone-DTR*: 16.08 ± 2.11 μm, in the simulation: 15.84 ± 0.98 μm, p = 0.73 by Mann–Whitney U test) and BC5i/o dendrites (distance to the farthest cone in *Cone-DTR*: 16.88 ± 0.95 μm, in the simulation: 15.20 ± 0.51 μm, p = 0.11 by Mann–Whitney U test) did not. These results underscore the cell-type specificity of homeostatic plasticity, reveal that dendritic remodeling precedes synaptic rewiring, and caution against interpreting dendritic remodeling as evidence for changes in synaptic connectivity.

Homeostatic plasticity of bipolar cell dendrites in mature mice

Neurodegeneration, including IRDs and AMD, primarily affects mature circuits [40,41]. We, therefore, wanted to test how homeostatic plasticity, which restored lost cone inputs to most bipolar cells in young retinas (Figure 3), changes with age. We labeled XBC, BC5i/o, BC6, and BC7 cells by intravitreal *AAV-Grm6-YFP* injection in P6 *Cone-DTR* and control mice, induced cone degeneration by intraperitoneal DT injection at P30, and isolated retinas for analysis at P60 (Figure 4A). At P30, synaptic connectivity and function of retinal circuits are mature and age-related degeneration is still in the distant future [35,42,43]. Across all types, more than 80% of bipolar cell dendrite tips in cones are synaptically differentiated and this fraction did not change after cone degeneration (Figure S6). As in young retinas, homeostatic plasticity of XBC dendrites precisely restored input synapses after cone loss in mature circuits (Figure 4B-D). This was accomplished within stable dendritic territories (Figure 4G) by increases in the fraction of cones contacted (Figure 4F) and the number of dendrite tips penetrating each cone (Figure 4E). By contrast, BC5i/o (Figure 4H-J), BC6 (Figure 4N-P), and BC7 cells (Figure 4T-V) failed to restore input synapse numbers to control levels when cone degeneration was induced at P30. For each type, the number of synapses per cone contacted was increased in *Cone-DTR* compared to control retinas (Figure 4E, K, Q, W). BC5i/o dendrites contacted more cones within their territory (Figure 4L) and BC6 dendrites expanded their reach (Figure 4S), but not vice versa (Figure 4M, R), and BC7 cells failed to significantly increase either the fraction of cones contacted with dendritic territories or the territories themselves (Figure 4, X, Y). Moreover, in the mature retina, short-term dendritic extension was restricted to BC6 cells (Figure S7).

Thus, the extent, mechanisms, and maturational decline of homeostatic plasticity of bipolar cells are cell-type specific (Figure 5). XBCs exhibit high homeostatic plasticity in young and mature retinas and restore inputs after cone degeneration by forming more synapses with a larger fraction of cones in stable dendritic fields. Homeostatic plasticity of BC5i/o and BC6

cells is high in young but low in mature retinas. In young retinas, BC5i/o and BC6 cells use different strategies to restore inputs. Whereas BC5i/o cells, like XBC, contact more cones within stable dendritic territories, BC6 cells expand dendritic territories to reach new cones. Both BC5i/o and BC6 form more synapses with each contacted cone after photoreceptor degeneration. In mature retinas, BC5i/o and BC6 cells retain differences in their homeostatic strategies but fail to restore synapses to pre-degeneration levels. Finally, BC7 cells employ a similar strategy to BC6 cells but are unable to recapture all synaptic input lost to cone degeneration in young or mature retinas.

Homeostatic plasticity and bipolar cell function

We found that homeostatic plasticity can precisely restore input synapse numbers of bipolar cells even when 50% of cones are lost to degeneration and that the capacity for such homeostasis declines with age (Figure 3, and Figure 4). To test whether homeostatic plasticity can restore bipolar cell function after cone degeneration and how functional recovery depends on age, we recorded *in vivo* electroretinograms (ERGs) in *Cone-DTR* and control mice at P40 and P60 following DT injection at P10 and P30, respectively. In dark-adapted flash ERGs, scotopic a- and b-waves were indistinguishable between DT-injected *Cone-DTR* and control mice at P40 (Figure 6A, B) and P60 (Figure 6G, H). Together with anatomical experiments (Figure 1M-U), this confirms that rods and rod bipolar cells are unaffected by cone degeneration in our model. In light-adapted flash ERGs, photopic b-waves were preserved after DT injection at P10 (Figure 6C, D) but strongly attenuated when cone degeneration was induced at P30 (Figure 6I, J). Similarly, responses to intermediate stimulus frequencies (5-15 Hz) in light-adapted flicker ERGs were intact after cone degeneration in young (Figure 6E, F) but not mature mice (Figure 6K, L). Photopic b-waves and flicker ERG responses at intermediate frequencies are mediated by ON cone bipolar cells [44]. To probe the function of OFF cone bipolar cells, we analyzed light-adapted flicker ERG responses to high-frequency stimuli (18-30 Hz) [44]. These responses were preserved after DT injections at P10 (Figure 6E, F) but diminished after DT injections at P30 (Figure 6K, L). Together, these findings suggest that homeostatic rewiring restores bipolar cell function after cone degeneration in young mice and that the maturational decline in homeostatic plasticity leads to functional deficits if cone degeneration occurs later. Flicker ERG results further suggest that OFF and ON cone bipolar cells exhibit similar age-dependent changes in homeostatic plasticity.

Homeostatic plasticity determines visual deficits from cone degeneration

Our structural and functional data indicated that homeostatic plasticity of bipolar cells could be a promising therapeutic target for IRDs and AMD. However, such targets are ultimately only meaningful if they can improve vision. We, therefore, tested whether the maturational changes in homeostatic plasticity of bipolar cells are accompanied by changes in visual deficits from cone degeneration. BC5i/o and BC7 cells provide excitatory input to the ON direction-selective circuit, which drives gaze-stabilizing eye movements and optokinetic responses via projections to the accessory optic system [33,45,46]. BC5i/o cells exhibited high homeostatic plasticity in young retinas and low plasticity in mature retinas, while BC7s exhibited low plasticity in young and mature retinas (Figure 3, Figure 4). We measured eye tracking movements in awake head-fixed mice looking at a drifting grating stimulus (Figure

7A). As in our anatomy and ERG experiments, we compared *Cone-DTR* and control mice injected with DT at P10 or P30 at P40 and P60, respectively. Eye-tracking movements were preserved when cone degeneration was induced in young mice (Figure 7B, C), but were reduced when the same degeneration occurred in mature mice (Figure 7F, G).

To evaluate visual performance in a perceptual task, we conducted visual cliff tests, in which mice step from a central ledge onto a plexiglass surface with a checkerboard pattern immediately (i.e., shallow side) or 61 cm (i.e., deep side) underneath it (Figure 7D). *Cone-DTR* and control mice injected with DT at P10 showed equally strong preferences for the shallow side at P40 (Figure 7E). By contrast, after P30 DT injections *Cone-DTR* mice at P60 stepped more frequently to the deep side than control mice (Figure 7H). These results identify the maturational decline in homeostatic plasticity of bipolar cells as a key contributor to visual deficits incurred from photoreceptor degeneration and indicate that restoring developmental plasticity to mature bipolar cells could help preserve vision in IRDs and AMD.

DISCUSSION

Homeostatic plasticity refers to the drive and mechanisms by which neurons return to an activity setpoint following a perturbation [1-3]. A wide range of perturbations elicits homeostatic responses that engage an equally wide range of mechanisms [1-3]. How the choice of compensatory mechanisms depends on the nature of the perturbation is unclear. Here, we find that structural input loss elicits structural remodeling and synapse formation of bipolar cell dendrites. Other studies have shown that perturbations of input activity and intrinsic excitability are compensated by changes in synapse strength and ion channel regulation [47-49]. Together, these observations suggest that homeostatic adjustments start, when possible, in the realm of the perturbation. We speculate that this helps organize and coordinate plasticity mechanisms into insult-specific responses [50].

We find that in response to partial input loss, cone bipolar cells upregulate their connectivity with the remaining cones and only rarely form synapses with rods. Similarly, after focal laser ablation of cones, S-cone bipolar cell dendrites extend away from the injury site to connect specifically with S-cones [25]. Yet, when all cones are dysfunctional, cone bipolar cell dendrites switch their synaptic allegiances to rods [39]. In the inner retina, ganglion cells that receive input from multiple ON bipolar cell types, reorganize connections with their established partners when the major input type is selectively removed [5] but shift connections to OFF bipolar cells when ON bipolar cells are removed more broadly [7]. Together with results in other systems [51], this suggests that synaptic specificity is hierarchical rather than absolute and that developmental preferences are preserved during homeostatic rewiring.

It is widely appreciated that the diverse neurons that comprise most brain areas follow type-specific cues and strategies to assemble into precisely-wired circuits [9,35]. By contrast, how the homeostatic mechanisms that maintain these circuits and govern their responses to injury and degeneration differ between neuron types is unclear. Here, we discover remarkable diversity in the mechanisms, extent, and maturational decline of homeostatic plasticity of

four closely related neuron types. XBC and BC5i/o cell dendrites contact a subset of cones within their reach and restore connectivity in stable territories following partial cone loss. By contrast, dendrites of BC6 and BC7 cells contact most or all the cones in their reach and expand to recruit new partners following partial cone loss. Thus, different wiring presets appear to influence rewiring strategies by imposing different limits on their homeostatic capacity.

Homotypic signals restrict bipolar cell dendrite size [4,52,53]. The observation that BC6 and BC7 dendrite territories expand while bipolar cell numbers remain constant after cone degeneration indicates that the drive to recruit synaptic input can overcome growth-restricting homotypic signals.

In young retinas, XBC, BC5i/o, and BC6 cells precisely restore input synapse numbers when half the cones degenerate. In mature retinas, only XBC cells retain this capacity. Although neuronal plasticity is thought to decline with age, whether this applies to homeostatic plasticity *in vivo* was not known [54]. Similar to the differences in the maturational decline of homeostatic plasticity we discover, the time course of dendrite development was previously shown to vary between bipolar cell types [35,55]. The mechanisms that define the time course of dendrite development and the shift from high to low plasticity remain to be identified. Our results indicate that it will be critical to study these mechanisms in a cell-type-specific manner.

The precise restoration of input synapse numbers on bipolar cell dendrites in young mice is accompanied by complete preservation of retinal light responses as well as reflexive and perceptual visual behaviors. Furthermore, the maturational decline in bipolar cell rewiring is accompanied by deficits in retinal light responses and visual behaviors following cone degeneration. Differences in responses downstream of bipolar cells may contribute to the changes in retinal light responses and visual behaviors, but the most parsimonious explanation for our results is that homeostatic rewiring of bipolar cell dendrites determines functional outcomes from photoreceptor degeneration. This identifies homeostatic plasticity, particularly reversing its maturational decline in bipolar cells, as a promising therapeutic target for vision rescue and restoration in IRDs and AMD [16,17].

The cell-type specificity of homeostatic plasticity raises concerns about pursuing mechanistic studies aimed at translation in mice. Fortunately, recent studies revealed that bipolar cell types and their molecular makeup are conserved between mice and primates [14]. Quantitative accuracy in the face of significant perturbations is a hallmark of homeostatic plasticity [4,5] and an attractive feature for therapeutic interventions, which can be difficult to dose especially when degeneration is inhomogeneous and progressive as in IRDs and AMD [56]. Consistent with previous observations [24], we find that bipolar cell axons are unaffected by cone degeneration in young and mature retinas, indicating that if the connectivity of photoreceptors with bipolar cells can be restored by homeostatic rewiring, downstream processing of visual information will be intact. Efforts to enhance homeostatic plasticity of bipolar cells are orthogonal to conventional approaches aimed at preserving or regenerating photoreceptors [57] and are expected to work synergistically with them, one increasing the number of light-responsive cells and the other optimizing the transmission

and processing of signals downstream. Beyond the retina, homeostatic plasticity may be an attractive target for increasing the functional resilience of circuits to a wide range of neurodegenerative diseases.

STAR METHODS

LEAD CONTACT AND MATERIALS AVAILABILITY

Information and requests for resources and reagents should be directed to and will be fulfilled by the Lead Contact, Daniel Kerschensteiner (kerschensteinerd@wustl.edu). All unique stable reagents generated in this study are available from the Lead Contact with a completed Materials Transfer Agreement.

EXPERIMENTAL MODEL AND SUBJECT DETAILS

Mice.—To ablate cones, we generated *Cone-DTR* mice by crossing a transgenic strain in which Cre recombinase is transcribed from the human red/green opsin promoter [27] to a line in which the diphtheria toxin receptor (DTR) is expressed from a ubiquitously active locus in a Cre-dependent manner [28]. We dissolved diphtheria toxin (DT, Sigma) in PBS and injected mice once intraperitoneally (i.p.) with 0.01 μg g^{-1} bodyweight at postnatal day 10 (P10) or 0.1 μg g^{-1} bodyweight at P30. Cre-negative littermates injected with DT served as controls. We used a *Grm6-tdTomato* transgenic line [34], in addition to viruses, to label ON bipolar cells sparsely. For optokinetic testing, head plates were glued to the skull using dental resin (Parkell) in mice anesthetized with ketamine (0.1 mg g^{-1} body weight) and xylazine (0.01 mg g^{-1} bodyweight). After surgery, mice could recover for at least one week before optokinetic testing. All procedures in this study were approved by the Animal Studies Committee of Washington University School of Medicine (Protocol # 20170033) and performed in accordance with the National Institutes of Health *Guide for the Care and Use of Laboratory Animals*. We observed no sex-specific differences in our results and therefore combined data from male and female mice.

METHOD DETAILS

Adeno-associated virus (AAV) production and injection.—We used *AAV-Grm6-YFP* [4,5], in which four concatenated repeats of a 200-bp fragment of the *Grm6* promoter drive expression of yellow fluorescent protein,-sparsely label ON bipolar cells. To produce AAV1/2 chimeric virions, we co-transfected HEK-293 cells with the *pAAV-Grm6-YFP* plasmid, and helper plasmids encoding Rep2s and the Caps for serotype 1 and serotype 2, respectively. Cells and supernatant were harvested at 48 hrs after transfection, and viral particles were purified using heparin affinity columns (Sigma). For intravitreal AAV injections, mouse pups (P6) were anesthetized on ice, and 200 nL *AAV-Grm6-YFP* delivered into the vitreous chamber using a Nanoject II injector (Drummond).

Tissue preparation and immunohistochemistry.—Mice were sacrificed with CO_2 and enucleated. We isolated retinas in HEPES-buffered mouse artificial cerebrospinal fluid ($mACSF_{HEPES}$) containing (in mM): 119 NaCl, 2.5 KCl, 2.5 $CaCl_2$, 1.3 $MgCl_2$, 1 NaH_2PO_4, 11 glucose, and 20 HEPES (pH adjusted to 7.37 with NaOH), flat-mounted them on membrane disks (HABGO1300, Millipore) and fixed for 30 min in 4% paraformaldehyde in

mACSF$_{HEPES}$. For immunostaining, retinal cups were embedded in 4% agarose and cut into 60 μm slices on a vibratome (VT1000A, Leica). Flat-mounted retinas were cryoprotected in 10% sucrose in phosphate-buffered saline (PBS) for 1 hr at RT, 20% sucrose in PBS for 1 hr at RT, and 30% sucrose in PBS overnight at 4 °C. After three freeze-thaw cycles, retinas were washed three times for 10 min in PBS at RT, blocked in 10% normal donkey serum (NDS) in PBS for 2 hr at RT, and incubated with primary antibodies in 5% NDS and 0.5% Triton X-100 in PBS for 5 days at 4 °C. The following primary antibodies were used in this study: chicken anti-GFP (1:1000, ThermoFisher, RRID:AB_2534023), rabbit anti-cone arrestin (CAR, 1:1000, Millipore, RRID:AB_1163387), rabbit anti-M-opsin (1:1000, Millipore, RRID:AB_177456), goat anti-S-opsin (1:500, Santa Cruz, RRID:AB_2158332), goat anti-cholineacetyltransferase (ChAT, 1:200, Millipore, RRID:AB_11213095), mouse anti-Gpr179 (1:500, Millipore, RRID:AB_2069582), sheep anti-mGluR6 (1:200, from Dr. K. Martemyanov) [58], mouse anti-CtBP2 (1:500, BD Biosciences, RRID:AB_399431), rabbit anti-DsRed (1:1000, BD Biosciences, RRID:AB_394264), and mouse anti-RFP (1:500, Abcam, RRID:AB_1141717). After incubation with primary antibodies, retinas were washed in PBS three times for 10 min at RT, and stained with secondary antibodies conjugated with DyLight 405 (1:1000, ThermoFisher, anti-rabbit IgG RRID:AB_1965945), Alexa 488 (1:1000, ThermoFisher, anti-chicken IgY RRID:AB_2534096, anti-mouse IgG RRID:AB_2534069, anti-rabbit IgG RRID:AB_2556546), Alexa 568 (1:1000, Thermo-Fisher, anti-rabbit IgG RRID:AB_2534017, anti-mouse IgG RRID:2534013), and Alexa 633 (1:1000, ThermoFisher, anti-goat IgG RRID:AB_2535739, anti-mouse IgG RRID:AB_2535768, anti-sheep RRID:AB_2535754) overnight at 4 °C and mounted in Vectashield medium (Vector Laboratories, RRID:AB_2336789) after three washes in PBS for 10 min at RT. DAPI was mixed with secondary antibodies to stain for nuclei.

Imaging and analysis.—Confocal images were acquired on an Fv1000 laser scanning microscope (LSM, Olympus) using a 60X 1.35 NA oil immersion objective. Image stacks of bipolar cell axons and dendrites were acquired at a voxel size of 0.066 μm - 0.3 μm or 0.082 μm - 0.3 μm (x/y - z-axis). Bipolar cell types were identified based on the morphology and stratification of their axon arbors relative to the ChAT bands in the IPL. Axon stratification profiles were analyzed using Fiji [59] and MATLAB (The Mathworks). The borders of the IPL with the inner nuclear layer (0% IPL depth) and the ganglion cell layer (100% IPL depth) were demarcated by the position of ChAT-positive somata. To identify dendritic synapses, super-resolution images (voxel size: 0.043 μm - 0.1 μm, x/y - z) were acquired on an LSM 800 microscope (Zeiss) with an AiryScan detector array. Bipolar cell dendrite tips containing postsynaptic receptor clusters stained for Gpr179 or mGluR6 were counted as synapses and their position relative to cone pedicles (cone arrestin) analyzed. To reconstruct the connectivity of individual bipolar cells, binary masks were generated by local thresholding of fluorescent signals of bipolar cell dendrites or axons in Amira (FEI). For axons, binary masks were used to isolate CtBP2-positive synaptic ribbons of the respective cell [4,34]. Bipolar cell axon and dendrite territories were defined as the areas of the smallest convex polygons to encompass the respective arbors in z-projections of image stacks from flat-mounted retinas. The cone contact ratio of a bipolar cell was defined as the number of cones contacted by the cell over the number of cones within its dendritic territory. To test if the transient dendrite extensions of BC5i/o and BC7 cells seven days after DT

injection at P10 recruited new cone partners, we compared the distance the farthest cone contacted for each bipolar cell in *Cone-DTR* retinas at P40 to the distance to the farthest cone contacted in a simulation in which cones were removed to the same extent from dendritic fields of bipolar cells in P40 control retinas. The distance the farthest cone contacted is decreased in the stimulation compared to the control data. If dendritic extensions reach new cones, they would counteract this trend. Indeed, for BC6 cells, which extend dendrites stably, the distance to the farthest cone was increased. However, for BC5i/o and BC7 cells results from *Cone-DTR* retinas matched simulations.

Electroretinograms (ERGs).—Thirty days after DT injections at P10 or P30, mice were dark adapted overnight, anesthetized with ketamine (0.1 mg g^{-1} body weight) and xylazine (0.01 mg g^{-1} body weight) and their pupils dilated with 1% atropine sulfate (Falcon Pharmaceuticals). Responses to brief white light flashes (<5 ms) were acquired from control and *Cone-DTR* mice using a UTAS Visual Electrodiagnostic Testing System (LKC Technologies). Recording electrodes embedded in contact lenses were placed over the cornea of both eyes, and mouse body temperature was maintained at 37 ± 0.5 °C throughout recordings with a heating pad controlled by a rectal temperature probe (FHC, Inc., Bowdoin, ME, USA). Flash ERG recordings were performed as previously described [4]. Briefly, four to ten responses were averaged at each light level. The a-wave was measured as the difference between the response minimum in the first 50 ms after flash onset and the voltage value at flash onset; and the b-wave amplitude was measured as the difference between a 15–25 Hz low to pass to filtered b-wave peak and the a-wave amplitude. Flicker ERG recordings were adapted from a previous protocol [44] and performed after flash ERGs. Responses to trains of brief flashes at 2.53 cdS m^{-2} with varying rates (5, 7, 10, 12, 15, 18, 20 and 30 Hz) were acquired without any background illumination. Responses to flicker stimuli were mean-subtracted with a sliding window equal to one stimulus interval and averaged across 30 repeats before amplitudes were measured. All ERG analyses were performed using scripts written in MATLAB.

Visual behaviors.—For optokinetic response testing, mice were dark-adapted for >2 hrs >1 week after head plate surgery and 30 days after DT injection. Mice were restrained and head-fixed in a custom holder. Visual stimuli were presented on monitor 16 cm from the mouse's left eye at a 45° angle to the long body axis. Stimuli covered 120° of the visual field in azimuth and 75° in elevation. Stimuli consisted of square-wave gratings (mean luminance at the cornea: 50.8 lx; contrast: 100%; spatial frequency: 20° cycle^{-1}) drifting at 10° s^{-1} in the tempo-nasal direction. Each trial consisted of 30 s of a uniform gray screen, 180 s of a drifting gratings, and another 30 s of a uniform gray screen. Three to five stimulus trials were recorded for each mouse. Eye movements were tracked under IR illumination (Edmund optics) using an ETL-200 eye tracking system (ISCAN Inc.). Eye tracking movements (ETMs) were analyzed as described before [39]. For visual cliff testing, mice were placed on a 3.8 x 1.7 cm ridge (height x width) across the center of a 56 x 41 cm platform (width x depth). On one side of the ridge a checkerboard pattern was immediately underneath the platform (i.e., the shallow side), on the other side an identical checkerboard pattern was 61 cm below the platform (i.e., the deep side). Mice were filmed with a USB

camera (720p, ELP or C310, Logitech) and their preference for stepping to the shallow vs. deep side measured across ten trials.

QUANTIFICATION AND STATISTICAL ANALYSIS

Statistics.—Statistical differences were evaluated using one- or two-way ANOVA, Mann-Whitney U tests, and bootstrapping as appropriate and specified in the figure legends. In the text, figures and figure legends population data are presented as mean ± SEM. In the figures, significance is indicated by asterisks as * $p < 0.05$, ** $p < 0.01$, and *** $p < 0.001$.

DATA AND CODE AVAILABILITY

The datasets obtained for this study are available from the Lead Contact (kerschensteinerd@wustl.edu) upon reasonable request.

Supplementary Material

Refer to Web version on PubMed Central for supplementary material.

ACKNOWLEDGMENTS

REFERENCES

1. Tien N-W, and Kerschensteiner D (2018). Homeostatic plasticity in neural development. Neural Dev. 13, 9. [PubMed: 29855353]

2. Turrigiano GG (2008). The self-tuning neuron: synaptic scaling of excitatory synapses. Cell 135, 422–435. [PubMed: 18984155]

3. Davis GW (2006). Homeostatic control of neural activity: from phenomenology to molecular design. Annu. Rev. Neurosci. 29, 307–323. [PubMed: 16776588]

4. Johnson RE, Tien N-W, Shen N, Pearson JT, Soto F, and Kerschensteiner D (2017). Homeostatic plasticity shapes the visual system's first synapse. Nat. Commun. 8, 1220. [PubMed: 29089553]

5. Tien N-W, Soto F, and Kerschensteiner D (2017). Homeostatic Plasticity Shapes Cell-Type-Specific Wiring in the Retina. Neuron 94, 656–665.e4. [PubMed: 28457596]

6. Tripodi M, Evers JF, Mauss A, Bate M, and Landgraf M (2008). Structural homeostasis: compensatory adjustments of dendritic arbor geometry in response to variations of synaptic input. PLoS Biol. 6, e260. [PubMed: 18959482]

7. Okawa H, Della Santina L, Schwartz GW, Rieke F, and Wong ROL (2014). Interplay of cell-autonomous and nonautonomous mechanisms tailors synaptic connectivity of converging axons in vivo. Neuron 82, 125–137. [PubMed: 24698272]

8. Johnson RE, and Kerschensteiner D (2014). Retrograde plasticity and differential competition of bipolar cell dendrites and axons in the developing retina. Curr. Biol. 24, 2301–2306. [PubMed: 25220059]

9. Shen K, and Scheiffele P (2010). Genetics and cell biology of building specific synaptic connectivity. Annu. Rev. Neurosci. 33, 473–507. [PubMed: 20367446]

10. Euler T, Haverkamp S, Schubert T, and Baden T (2014). Retinal bipolar cells: elementary building blocks of vision. Nat. Rev. Neurosci. 15, 507–519. [PubMed: 25158357]

11. Shekhar K, Lapan SW, Whitney IE, Tran NM, Macosko EZ, Kowalczyk M, Adiconis X, Levin JZ, Nemesh J, Goldman M, et al. (2016). Comprehensive Classification of Retinal Bipolar Neurons by Single-Cell Transcriptomics. Cell 166, 1308–1323.e30. [PubMed: 27565351]

12. Franke K, Berens P, Schubert T, Bethge M, Euler T, and Baden T (2017). Inhibition decorrelates visual feature representations in the inner retina. Nature 542, 439–444. [PubMed: 28178238]

13. Cronin TW, Johnsen S, Justin Marshall N, and Warrant EJ (2014). Visual Ecology (Princeton University Press).

14. Peng Y-R, Shekhar K, Yan W, Herrmann D, Sappington A, Bryman GS, van Zyl T, Do MTH, Regev A, and Sanes JR (2019). Molecular Classification and Comparative Taxonomics of Foveal and Peripheral Cells in Primate Retina. Cell. Available at: http://www.sciencedirect.com/science/article/pii/S0092867419300376.

15. Buch H, Vinding T, La Cour M, Appleyard M, Jensen GB, and Nielsen NV (2004). Prevalence and causes of visual impairment and blindness among 9980 Scandinavian adults: the Copenhagen City Eye Study. Ophthalmology 111, 53–61. [PubMed: 14711714]

16. Daiger SP, Sullivan LS, Bowne SJ, and Rossiter BJF (2019). RetNet: retinal information network. RetNet: retinal information network. Available at: https://sph.uth.edu/RetNet/.

17. Wright AF, Chakarova CF, Abd El-Aziz MM, and Bhattacharya SS (2010). Photoreceptor degeneration: genetic and mechanistic dissection of a complex trait. Nat. Rev. Genet 11, 273–284. [PubMed: 20212494]

18. Aït-Ali N, Fridlich R, Millet-Puel G, Clérin E, Delalande F, Jaillard C, Blond F, Perrocheau L, Reichman S, Byrne LC, et al. (2015). Rod-derived cone viability factor promotes cone survival by stimulating aerobic glycolysis. Cell 161, 817–832. [PubMed: 25957687]

19. Byrne LC, Dalkara D, Luna G, Fisher SK, Clérin E, Sahel J-A, Léveillard T, and Flannery JG (2015). Viral-mediated RdCVF and RdCVFL expression protects cone and rod photoreceptors in retinal degeneration. Journal of Clinical Investigation 125, 105–116. Available at: 10.1172/jci65654. [PubMed: 25415434]

20. Marc RE, Jones BW, Watt CB, and Strettoi E (2003). Neural remodeling in retinal degeneration. Prog. Retin. Eye Res 22, 607–655. [PubMed: 12892644]

21. Jones RS, Carroll RC, and Nawy S (2012). Light-induced plasticity of synaptic AMPA receptor composition in retinal ganglion cells. Neuron 75, 467–478. [PubMed: 22884330]

22. Chang B, Hawes NL, Hurd RE, Davisson MT, Nusinowitz S, and Heckenlively JR (2002). Retinal degeneration mutants in the mouse. Vision Res. 42, 517–525. [PubMed: 11853768]

23. Strettoi E, Pignatelli V, Rossi C, Porciatti V, and Falsini B (2003). Remodeling of second-order neurons in the retina of rd/rd mutant mice. Vision Res. 43, 867–877. [PubMed: 12668056]

24. Care RA, Kastner DB, De la Huerta I, Pan S, Khoche A, Della Santina L, Gamlin C, Santo Tomas C, Ngo J, Chen A, et al. (2019). Partial Cone Loss Triggers Synapse-Specific Remodeling and Spatial Receptive Field Rearrangements in a Mature Retinal Circuit. Cell Rep. 27, 2171–2183.e5. [PubMed: 31091454]

25. Beier C, Palanker D, and Sher A (2018). Stereotyped Synaptic Connectivity Is Restored during Circuit Repair in the Adult Mammalian Retina. Curr. Biol Available at: http://www.sciencedirect.com/science/article/pii/S0960982218305359.

26. Sher A, Jones BW, Huie P, Paulus YM, Lavinsky D, Leung L-SS, Nomoto H, Beier C, Marc RE, and Palanker D (2013). Restoration of retinal structure and function after selective photocoagulation. J. Neurosci 33, 6800–6808. [PubMed: 23595739]

27. Le Y-Z, Ash JD, Al-Ubaidi MR, Chen Y, Ma J-X, and Anderson RE (2004). Targeted expression of Cre recombinase to cone photoreceptors in transgenic mice. Mol. Vis 10, 1011–1018. [PubMed: 15635292]

28. Buch T, Heppner FL, Tertilt C, Heinen TJAJ, Kremer M, Wunderlich FT, Jung S, and Waisman A (2005). A Cre-inducible diphtheria toxin receptor mediates cell lineage ablation after toxin administration. Nat. Methods 2, 419–426. [PubMed: 15908920]

29. Haverkamp S, Wässle H, Duebel J, Kuner T, Augustine GJ, Feng G, and Euler T (2005). The primordial, blue-cone color system of the mouse retina. J. Neurosci 25, 5438–5445. [PubMed: 15930394]

30. Röhlich P, van Veen T, and Szél A (1994). Two different visual pigments in one retinal cone cell. Neuron 13, 1159–1166. [PubMed: 7946352]

31. Baden T, Schubert T, Chang L, Wei T, Zaichuk M, Wissinger B, and Euler T (2013). A tale of two retinal domains: near-optimal sampling of achromatic contrasts in natural scenes through asymmetric photoreceptor distribution. Neuron 80, 1206–1217. [PubMed: 24314730]

32. Helmstaedter M, Briggman KL, Turaga SC, Jain V, Seung HS, and Denk W (2013). Connectomic reconstruction of the inner plexiform layer in the mouse retina. Nature 500, 168–174. [PubMed: 23925239]

33. Greene MJ, Kim JS, Seung HS, and EyeWirers (2016). Analogous Convergence of Sustained and Transient Inputs in Parallel On and Off Pathways for Retinal Motion Computation. Cell Rep. 14, 1892–1900. [PubMed: 26904938]

34. Kerschensteiner D, Morgan JL, Parker ED, Lewis RM, and Wong ROL (2009). Neurotransmission selectively regulates synapse formation in parallel circuits in vivo. Nature 460, 1016–1020. [PubMed: 19693082]

35. Dunn FA, and Wong ROL (2012). Diverse strategies engaged in establishing stereotypic wiring patterns among neurons sharing a common input at the visual system's first synapse. J. Neurosci 32, 10306–10317. [PubMed: 22836264]

36. Behrens C, Schubert T, Haverkamp S, Euler T, and Berens P (2016). Connectivity map of bipolar cells and photoreceptors in the mouse retina. Elife 5 Available at: 10.7554/eLife.20041.

37. Orlandi C, Omori Y, Wang Y, Cao Y, Ueno A, Roux MJ, Condomitti G, de Wit J, Kanagawa M, Furukawa T, et al. (2018). Transsynaptic Binding of Orphan Receptor GPR179 to Dystroglycan-Pikachurin Complex Is Essential for the Synaptic Organization of Photoreceptors. Cell Rep. 25, 130–145.e5. [PubMed: 30282023]

38. Ray TA, Heath KM, Hasan N, Noel JM, Samuels IS, Martemyanov KA, Peachey NS, McCall MA, and Gregg RG (2014). GPR179 Is Required for High Sensitivity of the mGluR6 Signaling Cascade in Depolarizing Bipolar Cells. J. Neurosci 34, 6334–6343. [PubMed: 24790204]

39. Haverkamp S, Michalakis S, Claes E, Seeliger MW, Humphries P, Biel M, and Feigenspan A (2006). Synaptic plasticity in CNGA3(−/−) mice: cone bipolar cells react on the missing cone input and form ectopic synapses with rods. J. Neurosci 26, 5248–5255. [PubMed: 16687517]

40. Zayit-Soudry S, Duncan JL, Syed R, Menghini M, and Roorda AJ (2013). Cone structure imaged with adaptive optics scanning laser ophthalmoscopy in eyes with nonneovascular age-related macular degeneration. Invest. Ophthalmol. Vis. Sci 54, 7498–7509. [PubMed: 24135755]

41. Duncan JL, Pierce EA, Laster AM, Daiger SP, Birch DG, Ash JD, Iannaccone A, Flannery JG, Sahel JA, Zack DJ, et al. (2018). Inherited Retinal Degenerations: Current Landscape and Knowledge Gaps. Transl. Vis. Sci. Technol 7, 6.

42. Samuel MA, Voinescu PE, Lilley BN, de Cabo R, Foretz M, Viollet B, Pawlyk B, Sandberg MA, Vavvas DG, and Sanes JR (2014). LKB1 and AMPK regulate synaptic remodeling in old age. Nat. Neurosci 17, 1190–1197. [PubMed: 25086610]

43. van der List DA, and Chalupa LM (2006). Dendrites of rod bipolar cells sprout in normal aging retina. Proceedings of the. Available at: https://www.pnas.org/content/103/32/12156.short.

44. Tanimoto N, Sothilingam V, Kondo M, Biel M, Humphries P, and Seeliger MW (2015). Electroretinographic assessment of rod- and cone-mediated bipolar cell pathways using flicker stimuli in mice. Sci. Rep 5, 10731. [PubMed: 26029863]

45. Simpson JI (1984). THE ACCESSORY OPTIC SYSTEM. Annu. Rev. Neurosci 7, 13–41. [PubMed: 6370078]

46. Matsumoto A, Briggman KL, and Yonehara K (2019). Spatiotemporally Asymmetric Excitation Supports Mammalian Retinal Motion Sensitivity. Curr. Biol Available at: 10.1016/j.cub.2019.08.048.

47. Nerbonne JM, Gerber BR, Norris A, and Burkhalter A (2008). Electrical remodelling maintains firing properties in cortical pyramidal neurons lacking KCND2-encoded A-type K+ currents. J. Physiol 586, 1565–1579. [PubMed: 18187474]

48. Parrish JZ, Kim CC, Tang L, Bergquist S, Wang T, Derisi JL, Jan LY, Jan YN, and Davis GW (2014). Krüppel mediates the selective rebalancing of ion channel expression. Neuron 82, 537–544. [PubMed: 24811378]

49. Turrigiano GG, Leslie KR, Desai NS, Rutherford LC, and Nelson SB (1998). Activity-dependent scaling of quantal amplitude in neocortical neurons. Nature 391, 892–896. [PubMed: 9495341]

50. Marder E, and Tang LS (2010). Coordinating different homeostatic processes. Neuron 66, 161–163. [PubMed: 20434992]

51. Xu C, Theisen E, Maloney R, Peng J, Santiago I, Yapp C, Werkhoven Z, Rumbaut E, Shum B, Tarnogorska D, et al. (2019). Control of Synaptic Specificity by Establishing a Relative Preference for Synaptic Partners. Neuron. Available at: 10.1016/j.neuron.2019.06.006.

52. Lee SCS, Cowgill EJ, Al-Nabulsi A, Quinn EJ, Evans SM, and Reese BE (2011). Homotypic regulation of neuronal morphology and connectivity in the mouse retina. J. Neurosci 31, 14126–14133. [PubMed: 21976497]

53. Soto F, Tien N-W, Goel A, Zhao L, Ruzycki PA, and Kerschensteiner D (2019). AMIGO2 Scales Dendrite Arbors in the Retina. Cell Rep. 29, 1568–1578.e4. [PubMed: 31693896]

54. Takesian AE, and Hensch TK (2013). Balancing plasticity/stability across brain development. Prog. Brain Res 207, 3–34. [PubMed: 24309249]

55. Simmons AB, Bloomsburg SJ, Sukeena JM, Miller CJ, Ortega-Burgos Y, Borghuis BG, and Fuerst PG (2017). DSCAM-mediated control of dendritic and axonal arbor outgrowth enforces tiling and inhibits synaptic plasticity. Proc. Natl. Acad. Sci. U. S. A 114, E10224–E10233. [PubMed: 29114051]

56. Jones BW, Pfeiffer RL, Ferrell WD, Watt CB, Tucker J, and Marc RE (2016). Retinal Remodeling and Metabolic Alterations in Human AMD. Front. Cell. Neurosci 10, 103. [PubMed: 27199657]

57. Roska B, and Sahel J-A (2018). Restoring vision. Nature 557, 359–367. [PubMed: 29769667]

58. Cao Y, Masuho I, Okawa H, Xie K, Asami J, Kammermeier PJ, Maddox DM, Furukawa T, Inoue T, Sampath AP, et al. (2009). Retina-Specific GTPase Accelerator RGS11/G 5S/R9AP Is a Constitutive Heterotrimer Selectively Targeted to mGluR6 in ON-Bipolar Neurons. Journal of Neuroscience 29, 9301–9313. Available at: 10.1523/jneurosci.1367-09.2009. [PubMed: 19625520]

59. Schindelin J, Arganda-Carreras I, Frise E, Kaynig V, Longair M, Pietzsch T, Preibisch S, Rueden C, Saalfeld S, Schmid B, et al. (2012). Fiji: an open-source platform for biological-image analysis. Nat. Methods 9, 676–682. [PubMed: 22743772]

Highlights

- Cone degeneration elicits homeostatic rewiring of bipolar cell dendrites

- Homeostatic plasticity differs between bipolar cell types

- Homeostatic plasticity of bipolar cells declines steeply with age

- Homeostatic plasticity of bipolar cells determines visual function after cone loss
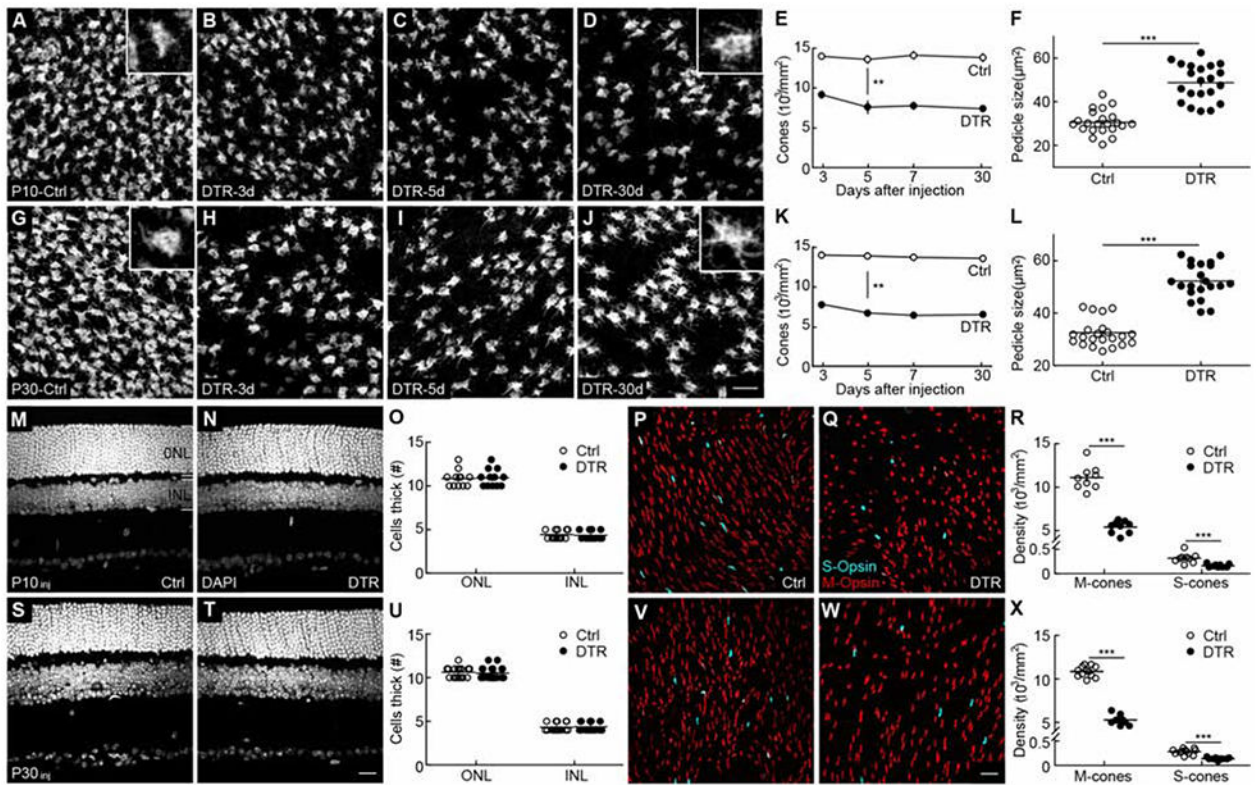
Figure 1. Transgenic model to precisely control cone degeneration.

(A-D) Representative images of cone pedicles with cone arrestin staining in control (A) and 3 (B), 5 (C), and 30 (D) days after DT injection at P10. Scale bar = 20 μm.

(E) Summary data for cone density in control (open circles) and *Cone-DTR* (filled circles) retina in (A-D). Cone density was lower in the *Cone-DTR* than in the control group (p = 4.9 x 10^{-21} by two-way ANOVA) and stable across time within each group (control, p = 0.84, *Cone-DTR*, p = 0.14 by one-way ANOVA, n = 3-5 mice and 5-7 images regions per mouse for each time point and genotype).

(F) Summary data for cone pedicle size in control (open circles) and *Cone-DTR* (filled circles) retinas 30 days after DT injection.

(G-J) Representative images of cone pedicles with cone arrestin staining in control (G) and 3 (H), 5 (I), and 30 (J) days after DT injection at P30. Scale bar = 20 μm.

(K) Summary data for cone density in control (open circles) and *Cone-DTR* (filled circles) retina in (G-J). Cone density was lower in *Cone-DTR* than in control retinas (p = 1.1 x 10^{-28} by two-way ANOVA) and stable across time within each group (control, p = 0.74, *Cone-DTR*, p = 0.27 by one-way ANOVA, n = 3-4 mice and 5-7 images regions per mouse for each time point and genotype).

(L) Summary data for cone pedicle size in control (open circles) and *Cone-DTR* (filled circles) retina at 30 days after DT injection.

(M, N, S, T) Representative images of vertical slices in control (M, S) and *Cone-DTR* (N, T) retinas 30 days after DT injection at P10 (M, N) and P30 (S, T) stained with DAPI. Scale bar = 20 μm.

(O, U) Summary data for outer nuclear layer (ONL) and inner nuclear layer (INL) thickness for P10 (O) and P30 (U) DT injections.

(P, Q, V, W) Representative images from dorsal regions of control (P and V) and *Cone-DTR* (V and W) retinas 30 days after DT injection at P10 (P, Q) and P30 (V, W) stained for M-opsin (red) and S-opsin (cyan). Scale bar = 20 μm.

(R, X) Summary data for M- and S-cone densities in control and *Cone-DTR* retinas after DT injection at P10 (R) and P30 (X). The ratio of M-/S-cones was unchanged in *Cone-DTR* compared-control retinas, indicating that cone removal affected both cells equally. Throughout this figure, absence of an asterisk indicates p 0.05, * indicates p < 0.05, ** indicates p < 0.01, and *** indicates p < 0.001. See also Table S1 and Figure S1.
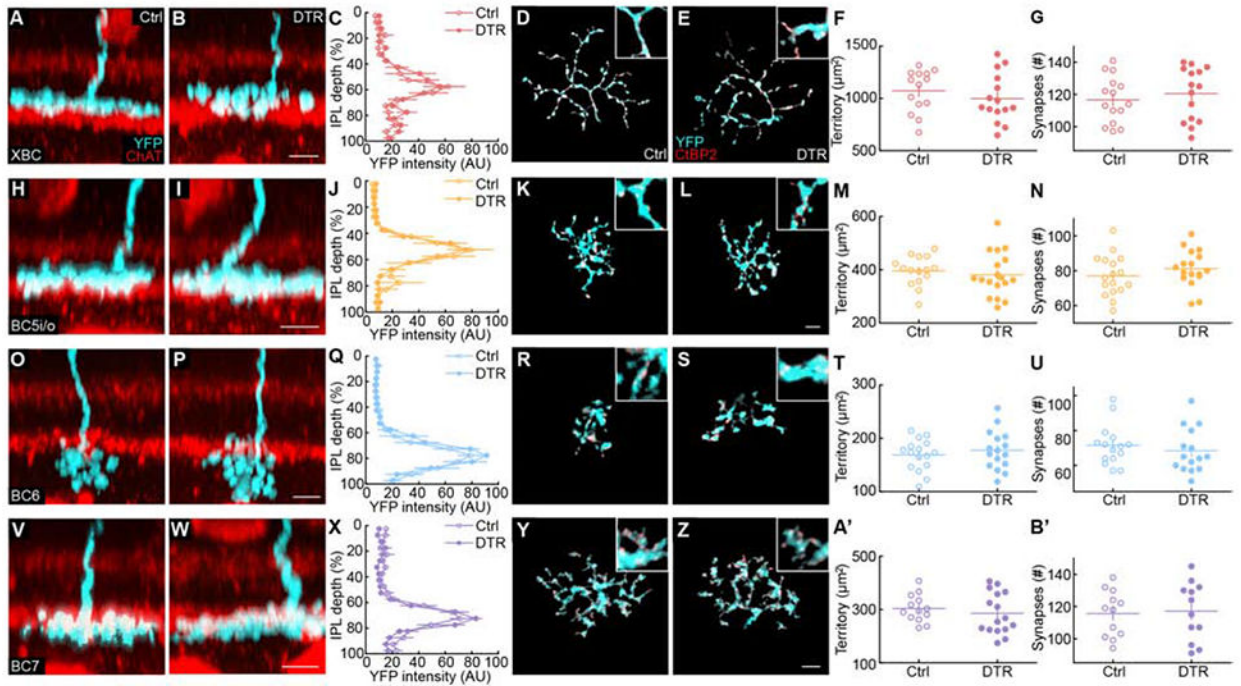
Figure 2. Bipolar cell axons remain stable after cone degeneration.

(A, B, H, I, O, P, V, W) Representative side view images for axons (cyan) of XBC (A, B), BC5i/o (H, I), BC6 (O, P) and BC7 (V, W) cell in control (A, H, O, V) and *Cone-DTR* (B, I, P, W) retinas 30 days after DT injection at P10 with choline acetylase (ChAT, red) staining for starburst amacrine cells.

(C, J, Q, X) Summary data of axon stratification profiles in control (open) and *Cone-DTR* (filled) for XBC (C), BC5i/o (J), BC6 (Q), and BC7 (X) cells.

(D, E, K, L, R, S, Y, Z) Representative images of maximum intensity projections for axons (cyan) of XBC (D, E), BC5i/o (K, L), BC6 (R, S), and BC7 (Y, Z) cells in control (D, K, R, Y) and *Cone-DTR* (E, L, S, Z) retinas 30 days after DT injection at P10. Ribbon release sites were stained for CtBP2 (red) and labeling associated with a single cell masked based on the image of its cytosolic fluorescence (YFP, cyan). Scale bar = 5 μm.

(F, G, M, N, T, U, A', B') Summary data for axonal territory (F, M, T, A') and number of synapses per axon (G, N, U, B') in control (open) and *Cone-DTR* (filled) XBCs (F,G), BC5i/o (M, N), BC6 (T, U), and BC7 (A', B') cells. Throughout this figure, absence of an asterisk indicates p   0.05. See also Table S2 and Figure S2.
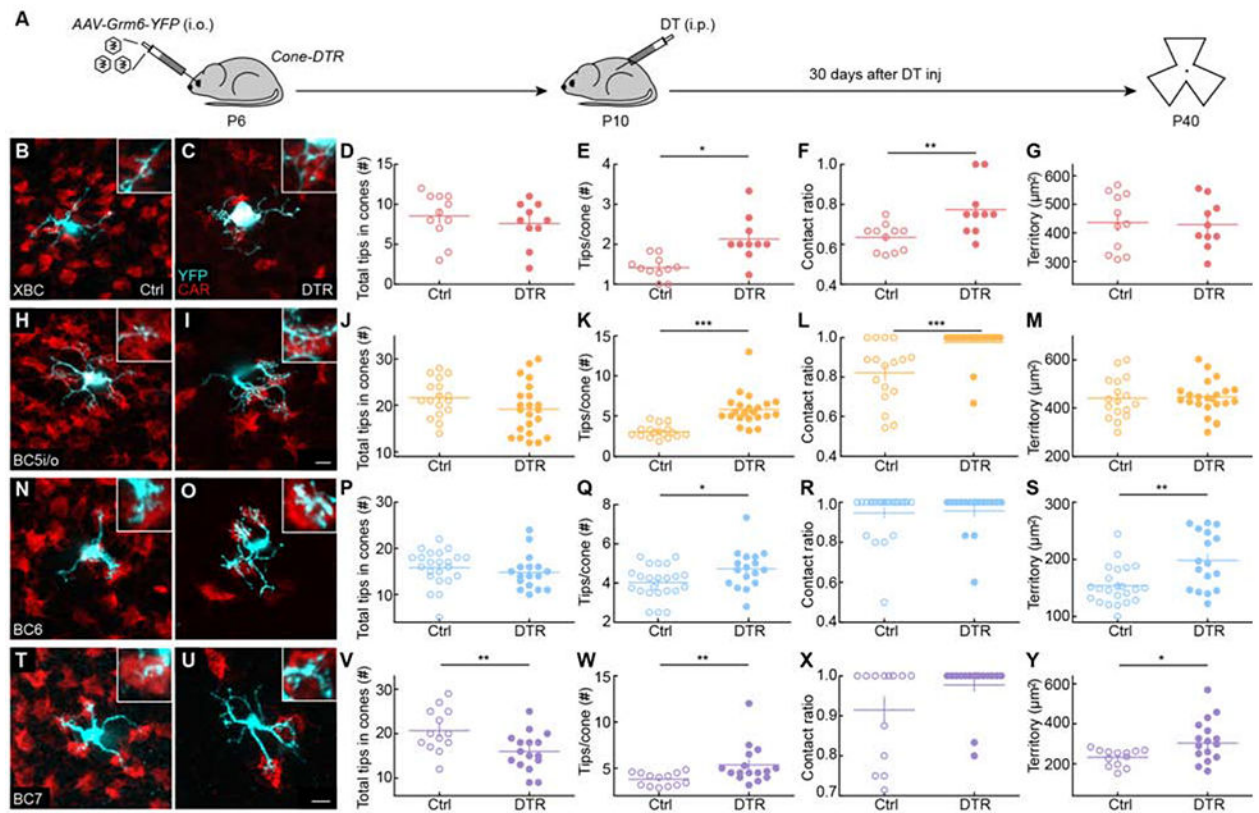
Figure 3. Homeostatic rewiring of bipolar cell dendrites after cone degeneration in young retinas.

(A) Timeline of the experiment. Mice were intravitreally injected with *AAV-Grm6-YFP* at P6 to label ON bipolar cells and intraperitoneally injected with diphtheria toxin (DT) once at P10 to ablate cones. Thirty days after DT injection (P40), retinas were dissected for analysis.

(B, C, H, I, N, O, T, U) Representative images of maximum intensity projections for dendrites (cyan) of XBC (B, C), BC5i/o (H, I), BC6 (N, O) and BC7 (T, U) cells in control (B, H, N, T) and *Cone-DTR* (C, I, O, U) retinas at 30 days after DT injection at P10 with cone arrestin (CAR, red) staining. Scale bar = 5 μm. Insets show higher magnification views of overlaps between dendritic tips and cones pedicles.

(D-G, J-M, P-S, V-Y) Summary data for total numbers of tips in cones (D, J, P, V), numbers of tips per cone (E, K, Q, W), contact ratios (F, L, R, X), and dendritic territories (G, M, S, Y) in control (open) and *Cone-DTR* (filled) XBCs (D-G), BC5i/o (J-M), BC6 (P-S), and BC7 (V-Y) cells. Throughout this figure, absence of an asterisk indicates p 0.05, * indicates p < 0.05, ** indicates p < 0.01, and *** indicates p < 0.001. See also Table S3 and Figures S3-S5.
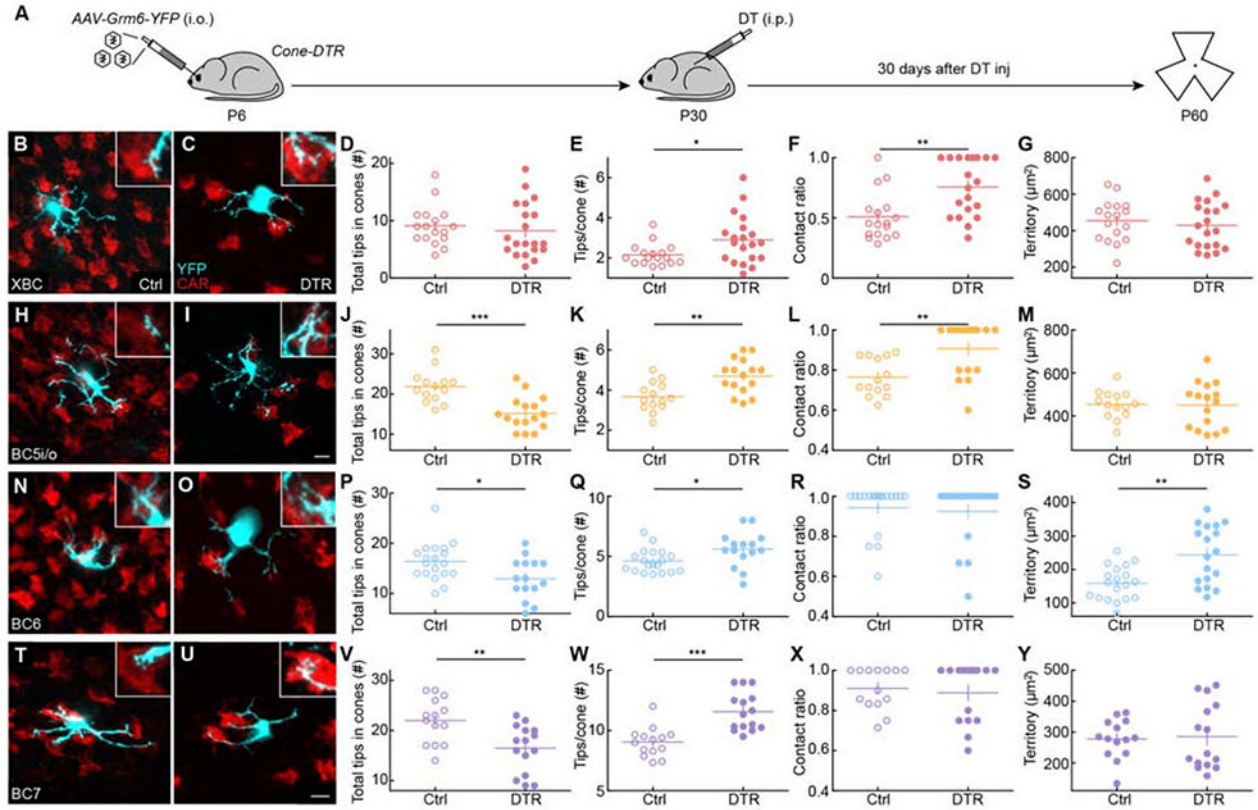
Figure 4. Limited homeostatic rewiring of bipolar cell dendrites after cone degeneration in mature retinas.

(A) Timeline of the experiment. Mice were intravitreally injected with *AAV-Grm6-YFP* at P6 to label ON bipolar cells and intraperitoneally injected with DT once at P30 to ablate cones. Thirty days after DT injection (P60), retinas were dissected for analysis.

(B, C, H, I, N, O, T, U) Representative images of maximum intensity projections for dendrites (cyan) of XBC (B, C), BC5i/o (H, I), BC6 (N, O), and BC7 (T, U) cells in control (B, H, N, T) and *Cone-DTR* (C, I, O, U) retinas 30 days after DT injection at P10 with cone arrestin (CAR, red) staining. Scale bar = 5 μm. Insets show higher magnification views of overlaps between dendritic tips and cones pedicles.

(D-G, J-M, P-S, V-Y) Summary data for total numbers of tips in cones (D, J, P, V), numbers of tips per cone (E, K, Q, W), contact ratios (F, L, R, X), and dendritic territories (G, M, S, Y) in control (open) and *Cone-DTR* (filled) XBCs (D-G), BC5i/o (J-M), BC6 (P-S), and BC7 (V-Y) cells. Throughout this figure, absence of an asterisk indicates p   0.05, * indicates p < 0.05, ** indicates p < 0.01, and *** indicates p < 0.001. See also Table S4 and Figures S6 and S7.
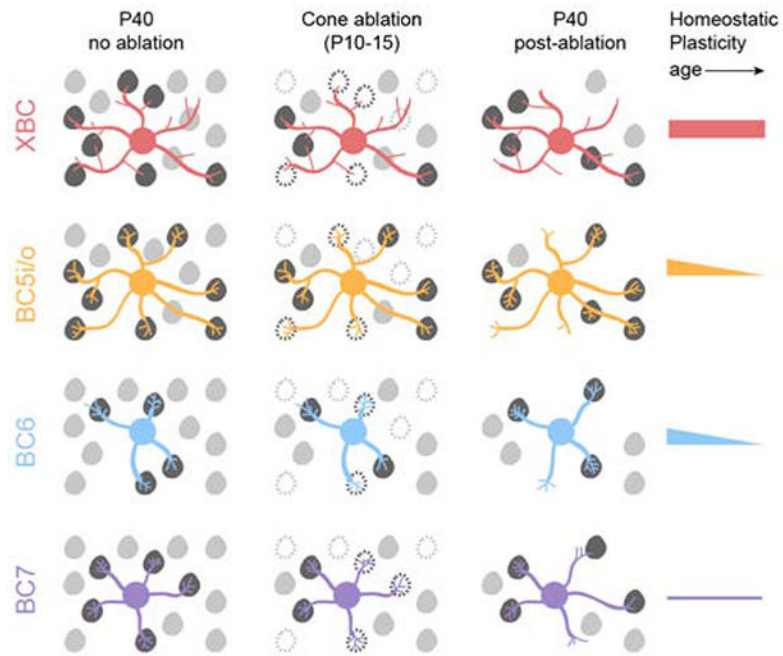
Figure 5. Homeostatic plasticity varies across bipolar cell types and age.
After cone degeneration, bipolar cells recover synaptic inputs by cell-type-specific strategies. XBC (red) and BC5i/o (orange) cells contact more cones within stable dendritic territories and form more contacts with each cone, whereas BC6 (blue) and BC7 (purple) cells expand dendritic territories to contact more cones and form more contacts with each cone. The extent and maturational decline in homeostatic plasticity also differs between bipolar cells with XBCs showing high plasticity in young and mature retinas, BC5i/o and BC6 cells showing high plasticity in young and low plasticity in mature retinas, and BC7 showing low plasticity in young and mature retinas.
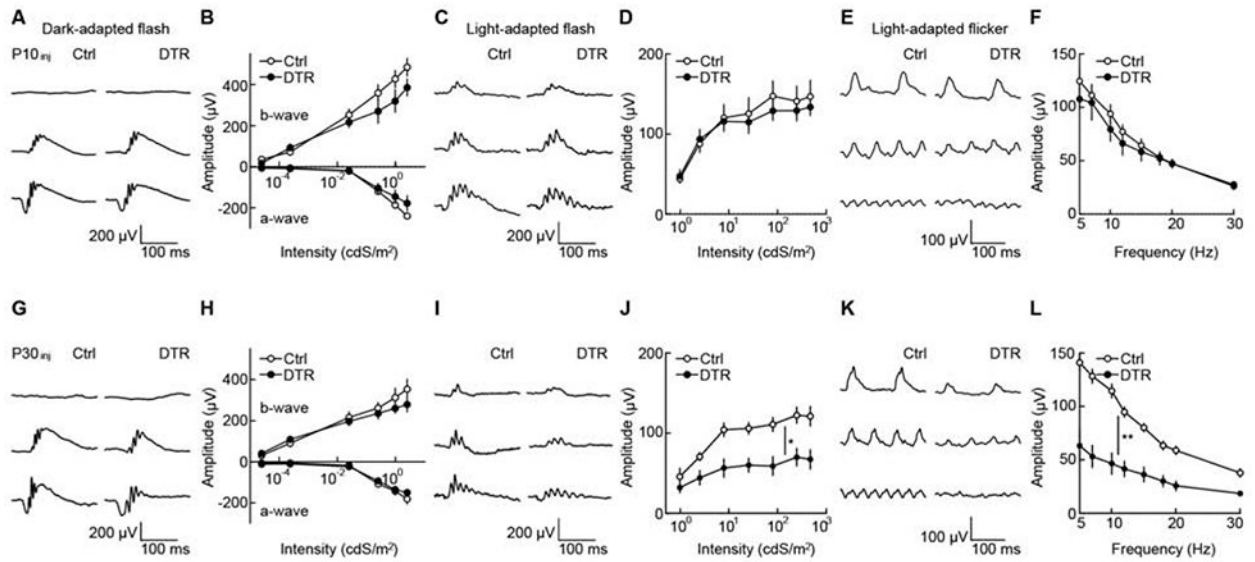
Figure 6. Age-dependent deficits in retinal light responses after cone degeneration.

(A, G) Representative traces for dark-adapted flash ERG responses to stimuli of increasing intensity (top row: 2.5×10^{-5} cdS m^{-2}, middle row: 2.52×10^{-2} cdS m^{-2}, bottom row: 9.83×10^{-1} cdS m^{-2}) in control (left column) and *Cone-DTR* (right column) mice 30 days after DT injection at P10 (A) and P30 (G).

(B, H) Summary data for intensity response functions of a- and b-wave amplitudes in control (open) and *Cone-DTR* (filled) mice after P10 (B) and P30 (H) DT injections.

(C, I) Representative traces for light-adapted flash ERG responses to stimuli of increasing light intensity (top row: 2.53 cdS m^{-2}, middle row: 25.49 cdS m^{-2}, bottom row: 470.28 cdS m^{-2}) in control (left column) and *Cone-DTR* (right column) mice 30 days after DT injection at P10 (C) and P30 (I).

(D, J) Summary data for intensity response functions of b-wave amplitudes in control (open) and *Cone-DTR* (filled) mice after P10 (D) and P30 (J) DT injections.

(E, K) Representative traces for light-adapted flicker ERG responses to stimuli of increasing frequency at 2.53 cdS m^{-2} (top row: 7 Hz, middle row: 15 Hz, bottom row: 30 Hz) in control (left column) and *Cone-DTR* (right column) mice 30 days after DT injection at P10 (E) and P30 (K).

(F, L) Summary data for intensity response functions in control (open) and *Cone-DTR* (filled) mice after P10 (F) and P30 (L) DT injections. Throughout this figure, absence of an asterisk indicates $p \ge 0.05$, * indicates $p < 0.05$, ** indicates $p < 0.01$, and *** indicates $p < 0.001$. See also Table S5.
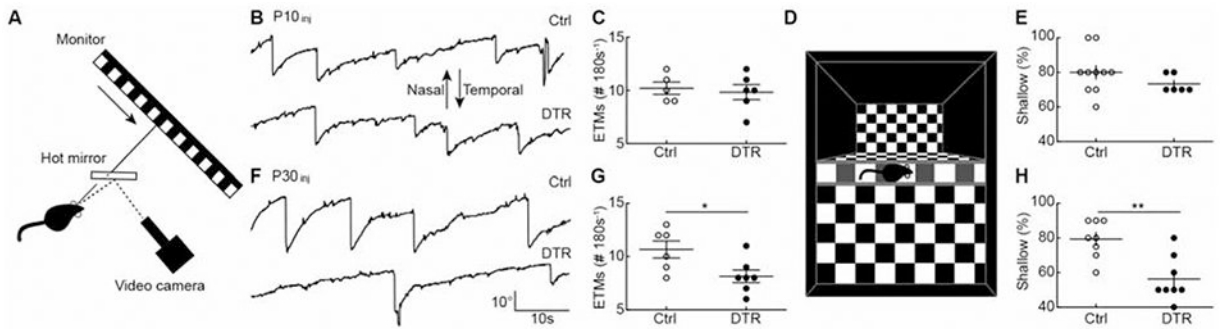
Figure 7. Age-dependent deficits in visual behaviors after cone degeneration.

(A) Schematic of the experimental setup for optokinetic testing. Drifting square-wave gratings (temporalnasal) were presented on a monitor 16 cm in front of the left eye. Movements of the left eye were recorded under IR illumination via a hot mirror.

(B, F) Representative eye movement traces for control (top) and *Cone-DTR* (bottom) mice 30 days after DT injection at P10 (B) and P30 (F).

(C, G) Summary data for eye tracking movements (ETMs) in control (open) and *Cone-DTR* (filled) mice 30 days after DT injection at P10 (C) and P30 (G).

(D) Illustration of the setup for visual cliff testing as described in STAR Methods.

(E, H) Summary data for percentage of shallow-side choices in control (open) and *Cone-DTR* (filled) mice 30 days after DT injection at P10 (E) and P30 (H). Throughout this figure, absence of an asterisk indicates p   0.05, * indicates p < 0.05, ** indicates p < 0.01, and *** indicates p < 0.001. See also Table S6.

KEY RESOURCES TABLE

REAGENT or RESOURCE	SOURCE	IDENTIFIER
Antibodies		
Goat anti-ChAT	Abcam	RRID:AB_2079595
Mouse anti-PKCα	Sigma	RRID:AB_477375
Mouse anti-Gαo	Millipore	RRID:AB_94671
Mouse anti-Syt2	Zebrafish International Resource Center	RRID:AB_10013783
Chicken anti-GFP	ThermoFisher	RRID:AB_2534023
Rabbit anti-DsRed	BD Biosciences	RRID:AB_394264
Mouse anti-RFP	Abcam	RRID:AB_1141717
Mouse anti-Gpr179	Millipore	RRID:AB_2069582
Rabbit anti-cone arrestin	Millipore	RRID:AB_1163387
Rabbit anti-M-opsin	Millipore	RRID:AB_177456
Goat anti-S-opsin	Santa Cruz	RRID:AB_2158332
Sheep anti-mGluR6	[58]	N/A
Mouse anti-CtBP2	BD Biosciences	RRID:AB_399431
Goat ant-rabbit IgG DyLight 405	ThermoFisher	RRID:AB_1965945
Donkey anti-chicken IgY Alexa 488	ThermoFisher	RRID:AB_2534096
Goat anti-mouse IgG Alexa 488	ThermoFisher	RRID:AB_2534084
Donkey ant-rabbit IgG Alexa 488	ThermoFisher	RRID:AB_2556546
Donkey anti-rabbit IgG Alexa 568	ThermoFisher	RRID:AB_2534017
Donkey anti-mouse IgG Alexa 568	ThermoFisher	RRID:AB_2534013
Donkey anti-goat IgG Alexa 633	ThermoFisher	RRID:AB_2535739
Goat anti-mouse IgG Alexa 633	ThermoFisher	RRID:AB_2535768
Donkey anti-sheep IgG Alexa 633	ThermoFisher	RRID:AB_2535754
Bacterial and Virus Strains		
AAV-Grm6-YFP	[4]	N/A
AAV-Grm6-tdTomato	[5]	N/A
Chemicals, Peptides, and Recombinant Proteins		
DAPI (4',6-Diamidino-2-Phenylindole, Dihydrochloride)	ThermoFisher	RRID:AB_2629482
Vectashield medium	Vector Laboratories	RRID:AB_2336789
Diphtheria toxin	Sigma	Cat# D0564
Experimental Models: Organisms/Strains		
Wild-type (C57Bl6/J)	Jackson Laboratory	RRID:IMSR_JAX:000664
B6;Tg(OPN1LW-cre)4Yzl (HRGP-Cre)	Jackson Laboratory	RRID:IMSR_JAX:032911
B6; Gt(ROSA)26Sortm1(HBEGF)Awai (iDTR)	Jackson Laboratory	RRID:IMSR_JAX:007900
Grm6-tdTomato	[34]	N/A
Software and Algorithms		
MATLAB	The Mathworks	RRID:SCR_001622

REAGENT or RESOURCE	SOURCE	IDENTIFIER
LKC	LKC Technologies	www.lkc.com
ISCAN	ISCAN Inc.	www.iscaninc.com
Fiji	[59]	RRID:SCR_002285
Amira	ThermoFisher	RRID:SCR_014305